

# Anomaly Discovery in Semantic Segmentation via Distillation Comparison Networks

Huan Zhou<sup>1,#</sup> Shi Gong<sup>1,#</sup> Yu Zhou<sup>1,†</sup> Zengqiang Zheng<sup>2</sup> Ronghua Liu<sup>2</sup> Xiang Bai<sup>1</sup>  
<sup>1</sup> Huazhong University of Science and Technology  
<sup>2</sup> Wuhan Jingce Electronic Group Co.,Ltd.

{huanzhou, gongshi, yuzhou, xbai}@hust.edu.cn {zhengzengqiang, liuronghua}@wuhanjingce.com

## Abstract

This paper aims to address the problem of anomaly discovery in semantic segmentation. Our key observation is that semantic classification plays a critical role in existing approaches, while the incorrectly classified pixels are easily regarded as anomalies. Such a phenomenon frequently appears and is rarely discussed, which significantly reduces the performance of anomaly discovery. To this end, we propose a novel Distillation Comparison Network (DiCNet). It comprises of a teacher branch which is a semantic segmentation network that removed the semantic classification head, and a student branch that is distilled from the teacher branch through a distribution distillation. We show that the distillation guarantees the semantic features of the two branches hold consistency in the known classes, while reflect inconsistency in the unknown class. Therefore, we leverage the semantic feature discrepancy between the two branches to discover the anomalies. DiCNet abandons the semantic classification head in the inference process, and hence significantly alleviates the issue caused by incorrect semantic classification. Extensive experimental results on StreetHazards dataset and BDD-Anomaly dataset are conducted to verify the superior performance of DiCNet. In particular, DiCNet obtains a 6.3% improvement in AUPR and a 5.2% improvement in FPR95 on StreetHazards dataset, achieves a 4.2% improvement in AUPR and a 6.8% improvement in FPR95 on BDD-Anomaly dataset. Codes are available at <https://github.com/zhouhuan-hust/DiCNet>.

## 1 Introduction

Semantic segmentation (Geng et al. 2021; Yuan and Wang 2018) aims to assign a semantic class label for each pixel. These approaches are trained on a set of known semantic classes. However, in the real world open scenario, if a pixel belongs to an unknown class, i.e., the never-seen-before class, it is dangerous to classify it into a predefined class instead of anomaly one. This paper focuses on exploiting Anomaly Discovery in Semantic Segmentation (ADSS), which aims to discover the pixels belonging to the unknown class. ADSS can be widely used in safety-critical applica-

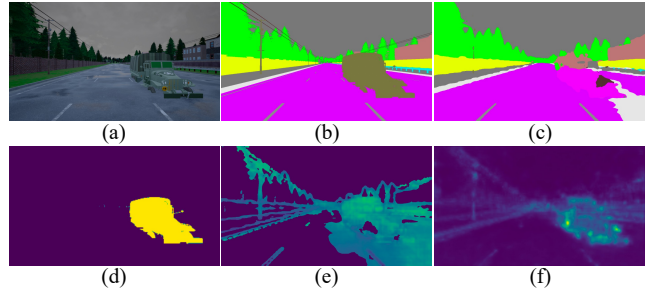


Figure 1: Comparison between SynthCP (Xia et al. 2020) and DiCNet. (a) is the input image, (b) is the ground truth of semantic segmentation, (c) is a semantic map predicted by PSPNet (Zhao et al. 2017), (d) is the ground truth of anomaly, (e) is the anomaly score map of SynthCP, (f) is the anomaly score map of DiCNet.

tions, such as autonomous driving (Janai et al. 2020), medical image analysis (Liu et al. 2019).

Given the input image shown in Fig. 1 (a), existing approaches firstly leverage a semantic segmentation network, e.g., PSPNet (Zhao et al. 2017), DeepLab (Chen et al. 2017), to predict a semantic map, as shown in Fig. 1 (c). Then they use different strategies to predict the anomalies based on the predicted semantic map. The uncertainty estimation based approaches (Hendrycks and Gimpel 2017; Hendrycks et al. 2019; Corbière et al. 2019) conduct different post-processing on the predicted semantic map, e.g., Softmax (Hendrycks and Gimpel 2017), CRF (Hendrycks et al. 2019), semantic map ensemble (Franchi et al. 2020; Gal and Ghahramani 2016; Izmailov et al. 2018; Lakshminarayanan, Pritzel, and Blundell 2017; Maddox et al. 2019; Vyas et al. 2018), to discover the anomalies. The image re-synthesis based methods (Lis et al. 2019; Xia et al. 2020; Di Biase et al. 2021) use the predicted semantic map to re-synthesis the original image, and compare the re-synthesis image with the original one to discover the anomalies. Hence, it is relatively apparent that semantic prediction is a core step in existing ADSS approaches.

**Our Finding:** *Since most of the existing approaches heavily depend on the semantic segmentation results, we observe*

# Equal contribution.

† Corresponding author.

| Method  | E-FPR95↓ | E-FPR85↓ | E-FPR75↓ |
|---------|----------|----------|----------|
| SynthCP | 85.2     | 72.8     | 62.3     |
| DiCNet  | 61.7     | 48.0     | 39.5     |
| Method  | C-FPR95↓ | C-FPR85↓ | C-FPR75↓ |
| SynthCP | 23.0     | 15.1     | 11.3     |
| DiCNet  | 13.4     | 8.6      | 6.3      |

Table 1: We decompose the normal pixels into two subsets, namely, the normal pixels that are correctly classified, and the normal pixels that are incorrectly classified. E-FPR95 measures how many incorrectly classified pixels are predicted as anomalies when the recall is 95%. C-FPR95 reflects how many correctly classified pixels are predicted as anomalies when the recall is 95%. We give the results of E-FPR and C-FPR at different recalls.

that the incorrectly classified pixels in semantic segmentation are easily regarded as anomalies. For instance, when compared with the ground truth given in Fig. 1 (b), the predicted semantic map in Fig. 1 (c) contains some incorrectly classified pixels, e.g., the pixels near the edge of the tree, the pixels inside the lower right corner region of the road. Accordingly, these pixels are predicted as anomalies by the existing state-of-the-art approach, i.e., SynthCP (Xia et al. 2020), as seen in Fig. 1 (e). The additional statistical analysis is reported in Tab. 1. For SynthCP, 85.2% of the incorrectly classified pixels are predicted as anomalies when the recall is 95% (E-FPR95), and the consistent conclusion can be observed at different recalls. Such a phenomenon seriously influences the accuracy of the anomaly discovery, while it is rarely discussed in existing approaches.

In this paper, we propose a Distillation Comparison Network (DiCNet) for anomaly discovery in semantic segmentation, which includes a teacher branch and a student branch. Both the teacher branch and the student branch are formed as a semantic segmentation network that removed the semantic classification head. The training phase of DiCNet includes two steps. The teacher branch is firstly trained under the common setting of the semantic segmentation, and then the student branch is distilled from the fixed teacher branch by the distribution distillation. The goal of the distillation is to guarantee that the teacher branch and the student branch hold consistency in the known classes, while reflect inconsistency in the unknown class. In the testing phase, we directly compare the output features of the teacher branch and the student branch. The discrepancy of these two branches is employed to assign an anomaly score for each pixel. As shown in Fig. 1 (f), DiCNet alleviates the issue caused by incorrect semantic classification efficiently. In addition, as shown in Tab. 1, DiCNet significantly reduces the E-FPR at different recalls. Furthermore, DiCNet also greatly reduces the C-FPR, which indicates that DiCNet is capable of produce fewer errors in the correctly classified pixels than SynthCP. We validate DiCNet on two challenging datasets, i.e., StreetHazards dataset and BDD-Anomaly dataset (Hendrycks et al. 2019) and show its superiority to existing ADSS approaches. To be specific, DiCNet achieves improvements over the state-of-the-art by 6.3% AUPR and

5.2% FPR95 on StreetHazards dataset, 4.2% AUPR and 6.8% FPR95 on BDD-Anomaly dataset.

To wrap up, the main contributions of this work lie in the following aspects:

- We give a deep study of the ADSS task, and reveal that the incorrectly classified pixels in semantic prediction are easily regarded as anomalies, leading to poor accuracy of ADSS. To the best of our knowledge, such an essential problem is rarely discussed in existing approaches.
- We customize a Distillation Comparison Network (DiCNet) to deal with the issue caused by the incorrectly classified pixels. DiCNet alleviates such a problem efficiently, and gains a significant improvement on two challenging datasets. Furthermore, DiCNet is simple and flexible.

## 2 Related Work

In this section, we briefly review the approaches about anomaly discovery in semantic segmentation and knowledge distillation, which are closely related to our approach.

### 2.1 Anomaly Discovery in Semantic Segmentation

Existing anomaly discovery in semantic segmentation approaches can be roughly classified into two categories, i.e., uncertainty estimation based approaches (Geifman and El-Yaniv 2017; Jiang et al. 2018; Vyas et al. 2018; Fontanel et al. 2021) and image re-synthesis based approaches (Lis et al. 2019; Xia et al. 2020; Di Biase et al. 2021).

**Uncertainty Estimation based Approaches.** These approaches first acquire a semantic prediction map by using a semantic segmentation network. (Hendrycks and Gimpel 2017) proposes the maximum softmax probability (MSP) to estimate the uncertainty of the semantic prediction, and the pixel with a higher uncertainty is regarded as an anomaly. However, as argued in (Corbière et al. 2019), the existing deep networks tend to produce a lower uncertainty for most of the pixels, which reduce the effectiveness of MSP. Hence (Corbière et al. 2019) proposes a true class probability for anomaly discovery, which improves the accuracy of MSP. In addition, recent approaches (Izmailov et al. 2018; Maddox et al. 2019) train multiple semantic segmentation networks, and estimate the uncertainty according to the variance of different semantic segmentation networks. (Gal and Ghahramani 2016) proposes the Monte Carlo Dropout to produce a set of semantic prediction results, but (Hendrycks et al. 2019; Lis et al. 2019) argue that MC Dropout fails to detect anomalies and produces a lot of false positives. (Lakshminarayanan, Pritzel, and Blundell 2017) proposes the ensemble models trained independently with different initialization seeds. (Franchi et al. 2020) proposes to compute the weight distributions, which can be used to sample an ensemble of networks for estimating the uncertainty.

**Image Re-synthesis based Approaches.** (Akçay, Atapour-Abarghouei, and Breckon 2018; Baur et al. 2018; Creusot and Munawar 2015; Munawar, Vinayavekhin, and De Magistris 2017) use autoencoder to segment the anomalies. They assume that the never-seen-before objects cannot be decoded

accurately. However, autoencoder tends to generate a lower-quality image. For the complex scenes with high variability in scene layout and lighting, they fail to find anomaly objects. (Lis et al. 2019; Xia et al. 2020; Di Biase et al. 2021) leverage a segmentation network (Badrinarayanan, Kendall, and Cipolla 2017; Zhao et al. 2017) to obtain the semantic map, then the generative network (Schlegl et al. 2017; Wang et al. 2018), such as GAN, is employed to learn a mapping from semantic map to the re-synthesis image. Since the re-synthesis image only contains the normal classes, the anomaly class can be discovered by comparing the re-synthesis image and the original one.

As we previously discussed, the semantic segmentation results exert a great impact on anomaly discovery in existing approaches, since the incorrectly classified pixels are easily regarded as anomalies. DiCNet alleviates this problem by comparing the discrepancy in feature space, which avoids errors caused by the semantic classification process.

## 2.2 Knowledge Distillation

Knowledge distillation aims to transfer the knowledge of a large network (a.k.a teacher network) to a small network (a.k.a student network). The student network may have an approximate predictive ability as the teacher network. Knowledge distillation methods can be divided into three types: logits-based approaches (Cho and Hariharan 2019; Hinton, Vinyals, and Dean 2015; Phuong and Lampert 2019; Xie et al. 2020; Yang et al. 2019; Zhang et al. 2018), feature-based approaches (Komodakis and Zagoruyko 2017; Romero et al. 2014), and relation-based approaches (Tung and Mori 2019; Yim et al. 2017; Romero et al. 2014). In this paper, we follow the feature-based paradigm (Romero et al. 2014) by proposing a distribution distillation. However, DiCNet is flexible since there are no strict constraints for the model size of the student branch.

## 3 Approach

In this section, we first formalize the anomaly discovery in semantic segmentation problem in Sec. 3.1, and then describe the specific network architecture in Sec. 3.2. The distribution distillation and the scoring rule are introduced in Sec. 3.3 and Sec. 3.4, respectively.

### 3.1 Problem Formulation

Given an input RGB image  $I \in \mathbb{R}^{H \times W \times 3}$ , the goal of anomaly discovery in semantic segmentation is to predict an anomaly score map  $A \in \mathbb{R}^{H \times W \times 1}$ . Each element of  $A$  indicates the probability that it belongs to the unknown class, i.e., the never-seen-before class. In the training phase, the pixel-level annotations of image  $I$  are given, and each pixel of  $I$  belongs to one of the  $Z$  semantic classes. The testing set contains  $Z + 1$  classes, and the pixels that belong to the additional unknown class are regarded as anomalies. They are assigned a high probability in  $A$ .

In this paper, we present a novel Distillation Comparison Network (DiCNet) for anomaly discovery in semantic segmentation. As illustrated in Fig. 2, the overall structure of DiCNet includes a teacher branch and a student branch (see

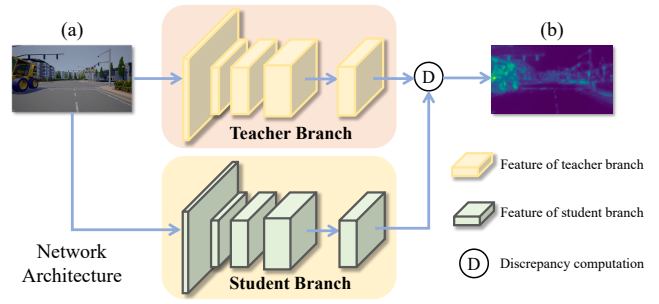


Figure 2: The network architecture of DiCNet. (a) is the input image. DiCNet contains a teacher branch and a student branch. The anomaly score is obtained by calculating the discrepancy between the two branches. (b) is the anomaly score map predicted by DiCNet.

Sec. 3.2). Both the teacher branch and the student branch are formed as a semantic segmentation network that removed the semantic classification head. The training phase of DiCNet is divided into two steps. The teacher branch is first trained under the common setting of the semantic segmentation, and then the student branch is distilled from the fixed teacher branch by using the distribution distillation (see Sec. 3.3). During the testing phase, the anomaly score of each pixel is assigned by the discrepancy of these two branches.

### 3.2 Network Architecture

**Teacher Branch.** In DiCNet, any semantic segmentation approach can be employed as the teacher branch, and the teacher branch is formulated as:

$$\mathbf{f}_t = \mathcal{U}(f_t) = \mathcal{U}(\theta_t(I)), \quad (1)$$

where  $\theta_t$  indicates the model parameter of the teacher branch, and  $f_t \in \mathbb{R}^{\frac{H}{8} \times \frac{W}{8} \times C}$  is the semantic features. Following (Xia et al. 2020), the ResNet-50 based PSPNet (Zhao et al. 2017) is used as the teacher branch in this paper. In addition,  $\mathcal{U}$  denotes the channel-wise normalization. Let  $f_t^c \in \mathbb{R}^{\frac{H}{8} \times \frac{W}{8} \times 1}$  denotes the  $c$ -th feature channel of  $f_t$ , where  $c \in \{1, 2, \dots, C\}$ . Since the values of  $f_t^c$  change in different ranges, it is not easy to distill its distribution. Therefore we calculate the mean  $m_t^c$  and the standard variance  $b_t^c$  of  $f_t^c$ , and then  $f_t^c$  is normalized as follows,

$$\mathbf{f}_t^c = \frac{f_t^c - m_t^c}{b_t^c}. \quad (2)$$

Through the observations on StreetHazards dataset (Hendrycks et al. 2019), we find that in each  $\mathbf{f}_t^c$ , the feature values of each semantic class fit a single Gaussian distribution, as shown in Fig. 3. Consequently,  $\mathbf{f}_t^c$  fits a Gaussian mixture distribution.

**Student Branch.** The student branch also receives  $I$  as the input, let  $\theta_s$  denotes the model parameter of the student branch, thus,

$$\mathbf{f}_s = \mathcal{U}(f_s) = \mathcal{U}(\theta_s(I)), \quad (3)$$

where  $\mathbf{f}_s \in \mathbb{R}^{\frac{H}{8} \times \frac{W}{8} \times C}$  is the output of the student branch. In the training phase, we want to optimize  $\theta_s$  to guarantee

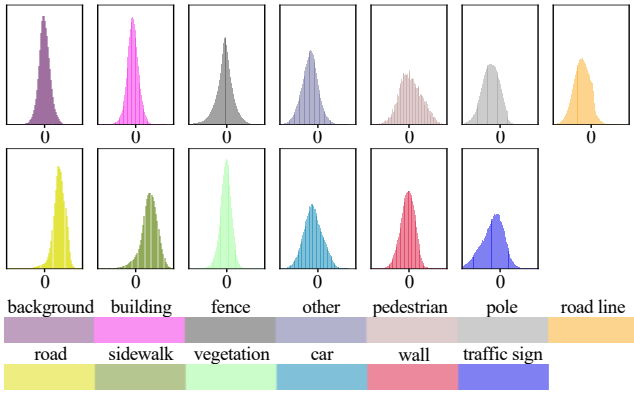


Figure 3: Numerical distribution of semantic features extracted from the training set of StreetHazards.

$\mathbf{f}_s$  and  $\mathbf{f}_t$  are as close as possible in the known  $\mathcal{Z}$  classes. Thus, we design the student branch that has a similar network structure as the teacher branch. In addition, different from existing knowledge distillation approaches (Cho and Hariharan 2019; Hinton, Vinyals, and Dean 2015; Phuong and Lampert 2019; Xie et al. 2020; Yang et al. 2019; Zhang et al. 2018; Komodakis and Zagoruyko 2017; Romero et al. 2014), which aim to distill the knowledge from a larger network to a smaller network. In our approach, the distillation is more flexible, since we can distill the knowledge from a fixed teacher network to any model size, e.g., we can distill the knowledge of a ResNet-50 based teacher branch to a ResNet-101 based student branch. We will experimentally demonstrate in Sec. 4.4 that, given a fixed teacher branch, DiCNet is less sensitive to the model size of the student branch. The accuracy difference between using different ResNet backbones is within 1%.

### 3.3 Distribution Distillation

Since we hope that  $\mathbf{f}_t$  and  $\mathbf{f}_s$  satisfy the same distribution in the known  $\mathcal{Z}$  classes, we define the discrepancy variable  $\mathbf{D} = \mathbf{f}_t \ominus \mathbf{f}_s$ , where  $\ominus$  denotes the element-wise subtraction, thus,  $\mathbf{D} \in \mathbb{R}^{\frac{H}{8} \times \frac{W}{8} \times C}$ . Based on Eq. (1),  $\mathbf{f}_t$  is the conditional distribution of  $I$  and  $\theta_t$ , which can be denoted as  $P(\mathbf{f}_t|I, \theta_t)$ .  $\mathbf{f}_s$  follows the same rules. Thus,

$$P(\mathbf{D}|\mathbf{f}_t, \mathbf{f}_s) = P(\mathbf{D}|I, \theta_t, \theta_s) \quad (4)$$

Therefore, each element  $d_{i,j}^c \in \mathbf{D}$  satisfies a Gaussian distribution, i.e.,  $d_{i,j}^c \sim \mathcal{N}(\mu^c, (\sigma^c)^2)$ . In the limit case, iff  $\mathbf{f}_t = \mathbf{f}_s$ ,  $\mathbf{D} = 0$ , and each element  $d_{i,j}^c \in \mathbf{D}$  is equal to 0. In such condition,  $\mu^c = 0$ ,  $\sigma^c = 0$ , and  $d_{i,j}^c$  satisfies the Dirac delta function. Such a phenomenon demonstrates that the student branch predicts the same results as the teacher branch in the known  $\mathcal{Z}$  classes. Therefore, the goal of the distribution distillation is to optimize the parameter  $\theta_s$  to minimize  $|\mu^c|$  and  $\sigma^c$ . Since we have the following equivalence relation,

$$\mu^c = 0, \sigma^c = 0 \iff \mathbf{D} = 0 \iff \mathbf{f}_t = \mathbf{f}_s \quad (5)$$

we can minimize each element  $d_{i,j}^c \in \mathbf{D}$  as follows,

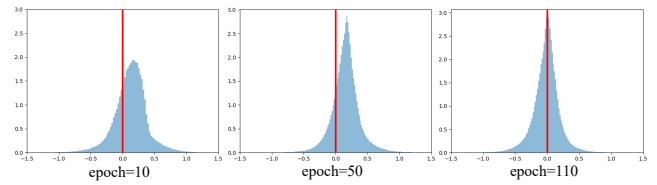


Figure 4: The distribution variations of  $d_{i,j}^c$  at different training epoch. (The backbone of teacher branch is ResNet-50, and the backbone of student branch is ResNet-34).

$$\mathcal{L} = \frac{1}{M \times C} \sum_{i,j,c} (d_{i,j}^c)^2. \quad (6)$$

where  $M$  denotes the mini-batch size. Since reducing  $d_{i,j}^c$  is equivalent to reduce  $\sigma^c$  and move  $\mu^c$  to 0, the distribution of  $d_{i,j}^c$  is inconsistent at different epoch. As shown in Fig. 4, when using a ResNet-50 based teacher branch, and a ResNet-34 based student branch. At epoch 10, the mean  $\mu^c$  deviates from 0, and the standard deviation  $\sigma^c$  is large. At epoch 50, the standard deviation  $\sigma^c$  becomes smaller, while the mean  $\mu^c$  still deviates from 0. At epoch 110, the mean  $\mu^c$  is close to 0. We should emphasize that the optimization process cannot guarantee that  $\mu^c$  achieves the limitation case, i.e.,  $\mu^c$  is strictly equal to 0. Hence, each channel may have an individual  $\mu^c$ . In addition, we observe that, by using a fixed teacher branch, the convergence speed of the distillation is related to the selection of the backbone. A larger backbone may lead to a faster convergence, while a smaller backbone needs more training epochs. However, it is fairly straightforward that a larger backbone may increase the inference time. Therefore, we can choose the best structure of DiCNet by jointly considering the accuracy, the convergence speed, and the inference time. More detailed results and discussions are given in Sec. 4.4.

### 3.4 Scoring Rule

Given a test image  $I$ , we input it into both the teacher branch and the student branch, and compute the discrepancy  $\mathbf{D}$ . As we discussed in Sec. 3.3, through the distribution distillation process, each element  $d_{i,j}^c \in \mathbf{D}$  satisfies a Gaussian distribution in the known  $\mathcal{Z}$  classes, while obeys a random distribution in the unknown class. Based on this observation, we define the anomaly score  $a_{i,j} \in \tilde{A}$  as the channel-wise variance of  $d_{i,j}^c$ :

$$a_{i,j} = \frac{1}{C} \sum_c (d_{i,j}^c - \mu^c)^2 \quad (7)$$

where  $\tilde{A} \in \mathbb{R}^{\frac{H}{8} \times \frac{W}{8} \times 1}$ . The intuitive motivation of Eq. (7) is that, if each  $d_{i,j}^c \sim \mathcal{N}(\mu^c, (\sigma^c)^2)$ ,  $d_{i,j}^c$  may be close to  $\mu^c$  in the known  $\mathcal{Z}$  classes, and hence,  $a_{i,j}$  may get a small anomaly score. In contrast, if  $d_{i,j}^c$  presents an arbitrary value that does not obey the learned Gaussian distribution, a larger score is assigned to  $a_{i,j}$  according to Eq. (7), which is regarded as an anomaly in this condition. In addition, in most cases, the Gaussian distribution and the random distribution are inseparable in a single channel. Thus, channel number  $C$  plays an important role in separating the anomaly from the

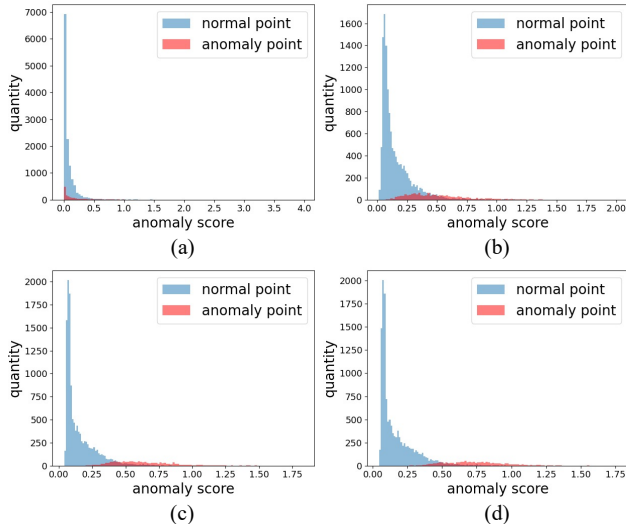


Figure 5: Anomaly score distribution with different channel number. (a)  $C = 1$ , (b)  $C = 10$ , (c)  $C = 100$ , (d)  $C = 512$ .

normal regions. As shown in Fig. 5, when  $C = 1$ , the value of the anomaly points (red points in Fig. 5 (a)) and normal points (blue points in Fig. 5 (a)) are mixed together. When we increase  $C$  to 10, a few anomalies show separability in terms of the feature value. As the channel number continues to increase, the overlap between the normal scores and the anomalies scores becomes smaller, e.g., when  $C = 512$ , most of the anomalies can be separated out. Finally,  $\tilde{A}$  is upsampled 8 times to achieve the anomaly score map  $A$ .

## 4 Experiments

### 4.1 Implementation Details

**Model Training.** DiCNet is implemented in PyTorch on Intel(R) Xeon(R) CPU and 4 NVIDIA TITAN Xp GPUs. Both the teacher branch and the student branch adopts a modified ResNet backbone pre-trained on ImageNet (Deng et al. 2009). The results reported in Tab. 1, Tab. 2 and Tab. 3 use ResNet-50 in teacher branch and ResNet-34 in student branch. More discussions about the selection of different backbones are given in Sec. 4.4. For training the teacher branch, the mini-batch size is set to 2. For training the student branch, the mini-batch size is set to 4. For StreetHazards dataset, We first train the teacher branch for 23 epochs with SGD using a learning rate of  $2 \times 10^{-2}$ , momentum of 0.9, and learning rate decay of  $10^{-4}$ . Next, in the student branch training phase, the weights of teacher branch are frozen, student branch is trained for 110 epochs with Adam ( $\beta_1 = 0.9$ ,  $\beta_2 = 0.999$ ) optimizer. We use a learning rate of  $10^{-4}$  and weight decay of  $10^{-5}$ . For BDD-Anomaly dataset, We first train the teacher branch for 19 epochs with SGD with momentum using a learning rate of  $2 \times 10^{-2}$ , momentum of 0.9, and learning rate decay of  $10^{-4}$ . Next, in the student branch training phase, the weights of teacher branch are frozen, student branch is trained for 160 epochs with Adam ( $\beta_1 = 0.9$ ,  $\beta_2 = 0.999$ ) optimizer. The initial learning rate is

| Method              | AUPR $\uparrow$ | FPR95 $\downarrow$ | AUROC $\uparrow$ |
|---------------------|-----------------|--------------------|------------------|
| MC Dropout(2016)    | 7.5             | 79.4               | 69.9             |
| MSP(2017)           | 6.6             | 33.7               | 87.7             |
| Deep Ensemble(2017) | 7.2             | 25.4               | 90.0             |
| AutoEncoder(2018)   | 2.2             | 91.7               | 66.1             |
| MSP+CRF(2019)       | 6.5             | 29.9               | 88.1             |
| TRADI(2020)         | 7.2             | 25.3               | 89.2             |
| SynthCP(2020)       | <b>9.3</b>      | 28.4               | 88.5             |
| PAnS(2021)          | 8.8             | <b>23.2</b>        | <b>91.1</b>      |
| <b>DiCNet</b>       | <b>15.6</b>     | <b>18.0</b>        | <b>93.3</b>      |

Table 2: Anomaly discovery results on StreetHazards dataset (Hendrycks et al. 2019).

set to  $10^{-4}$  and the learning rate drops by 0.1 at the 65th epoch. The weight decay is set to  $10^{-5}$ .

**Datasets.** StreetHazards (Hendrycks et al. 2019) leverages simulation to provide diverse, realistically-inserted anomaly objects, containing 5125 training images, 1031 validation images, and 1500 testing images. The image resolution is  $1280 \times 720$ . There are 250 types of anomaly objects appearing only in the testing images, and they are regarded as a single anomaly class. BDD-Anomaly (Hendrycks et al. 2019) is a large-scale dataset with diverse driving conditions derived from the BDD100K semantic segmentation dataset (Yu et al. 2020). The dataset contains 6,688 training images, 951 validation images without anomalies, and 361 testing images with anomalies. The image resolution is  $1280 \times 720$ . There are only two anomaly types, including motorcycle and train, and they are regarded as a single anomaly class.

**Evaluation Metrics.** Following (Hendrycks et al. 2019; Hendrycks and Gimpel 2017), we evaluate the performance of anomaly discovery by three metrics: Area Under the ROC curve (AUROC), False Positive Rate at 95% Recall (FPR95), Area Under the Precision-Recall curve (AUPR). Among these three metrics, we consider anomaly pixels to be positive and all the others to be negative.

**Baselines.** We compare our method to MC Dropout (Gal and Ghahramani 2016), MSP (Hendrycks and Gimpel 2017), Deep Ensemble (Lakshminarayanan, Pritzel, and Blundell 2017), AutoEncoder (Baur et al. 2018), MSP+CRF (Hendrycks et al. 2019), TRADI (Franchi et al. 2020), SynthCP (Xia et al. 2020) and PAnS (Fontanel et al. 2021). The AutoEncoder method is firstly proposed for anomaly segmentation in medical images, which do not need semantic labels. All other methods are specifically designed for semantic segmentation.

### 4.2 Quantitative Results

Tab. 2 shows the quantitative comparisons on the StreetHazards dataset. DiCNet outperforms all other methods in three metrics. In particular, in FPR95, DiCNet achieves an improvement of 5.2% (From 23.2% to 18.0%), which indicates that when the recall is fixed at 95%, DiCNet has a lower false positive rate than existing approaches. As previously mentioned in Tab. 1, the key improvement is induced by reducing the C-FPR and E-FPR. DiCNet improves the previous state-of-the-art approach SynthCP from 9.3% to 15.6% in terms

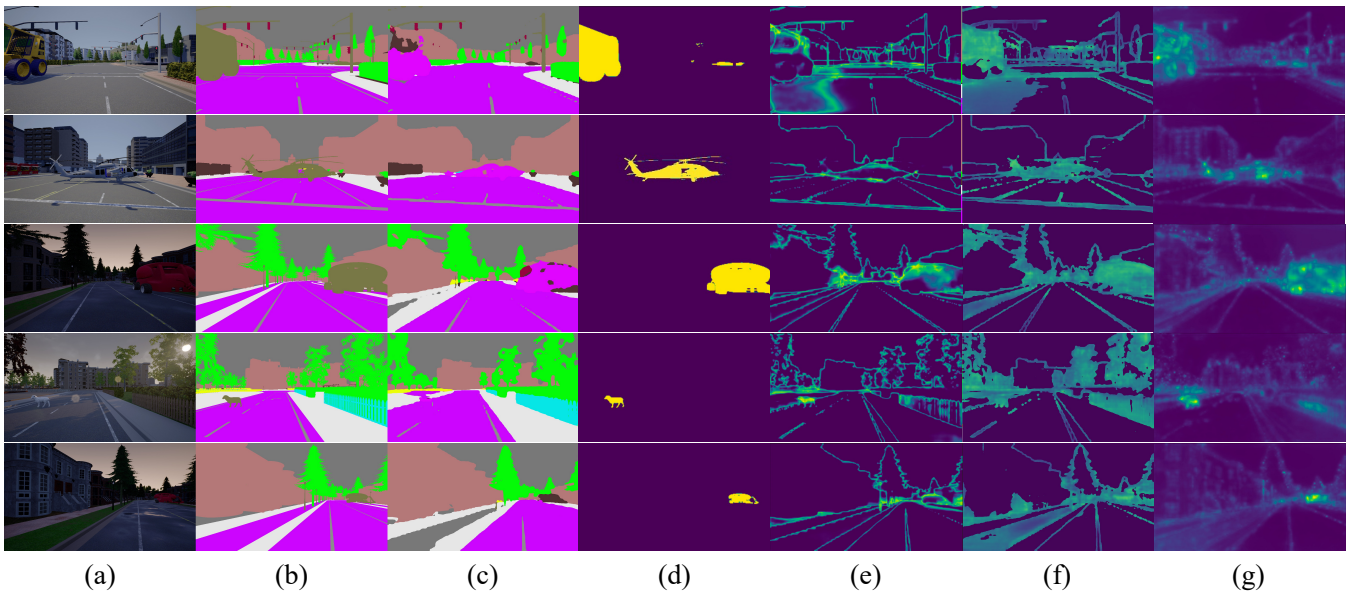


Figure 6: Qualitative comparisons with existing representative approaches. (a) the input images, (b) the ground truth of semantic segmentation, (c) the predicted semantic maps, (d) the ground truth of anomaly, (e) anomaly score maps of MSP (Hendrycks and Gimpel 2017), (f) anomaly score maps of SynthCP (Xia et al. 2020), (g) anomaly score maps of DiCNet. Best view in color.

| Method              | AUPR $\uparrow$ | FPR95 $\downarrow$ | AUROC $\uparrow$ |
|---------------------|-----------------|--------------------|------------------|
| MC Dropout(2016)    | 6.5             | 33.4               | 83.7             |
| MSP(2017)           | 6.3             | 31.9               | 84.2             |
| Deep Ensemble(2017) | 6.0             | <b>25.0</b>        | <b>87.0</b>      |
| AutoEncoder(2018)   | 1.4             | 82.2               | 56.8             |
| MSP+CRF(2019)       | <b>8.2</b>      | 26.0               | 86.3             |
| TRADI(2020)         | 5.6             | 26.9               | 86.1             |
| <b>DiCNet</b>       | <b>12.4</b>     | <b>18.2</b>        | <b>91.9</b>      |

Table 3: Anomaly discovery results on BDD-Anomaly dataset (Hendrycks et al. 2019).

of AUPR. For AUROC, DiCNet also achieves an improvement of 2.2% compared with existing methods. Tab. 3 shows the quantitative comparisons between our method and prior methods on the BDD-Anomaly dataset. As is known, BDD-Anomaly is a challenging dataset since many anomaly objects have a small size. Even under such circumstances, DiCNet achieves a 6.8% improvement in FPR95 and 4.2% improvement in AUPR, which significantly outperform other state-of-the-art approaches.

### 4.3 Qualitative Analysis

Fig. 6 illustrates the qualitative comparisons between MSP (Hendrycks and Gimpel 2017), SynthCP (Xia et al. 2020) and DiCNet. Given the input image shown in Fig. 6 (a), MSP, SynthCP and DiCNet use PSPNet (Zhao et al. 2017) to predict the semantic class of each pixel, which produces the results shown in Fig. 6 (c). Compared with the ground truth in Fig. 6 (b), the pixels around the edges are easily incorrectly classified, e.g., the pixels near the edge of a tree. As seen in Fig. 6 (e), MSP tends to assign a higher

anomaly score to the pixels near the edges. Similarly, in Fig. 6 (f), SynthCP also reports some anomalies near the edges. These visualizations clearly reflect that both MSP and SynthCP suffer from the presence of incorrectly classified pixels. Such a phenomenon corresponds to a higher E-FPR scores reported in Tab. 1. In addition, some correct classified pixels are still assigned a high anomaly score by MSP and SynthCP. Such a phenomenon can also be observed in the C-FPR scores in Tab. 1. In contrast, as we observed in Fig. 6 (g), DiCNet assigns a much lower anomaly score to the incorrectly classified pixels, e.g., the pixels around the edges, which corresponds to a lower false positive rate given in Tab. 1 and Tab. 2. Such results intuitively demonstrate that DiCNet is capable of effectively alleviating the essential problem caused by incorrect semantic classification. In addition, in the correct classified regions, DiCNet produces fewer anomalies. Such results reflect the reason for the improvement in C-FPR. Furthermore, when we compare the anomaly maps in the first row with the ground truth shown in Fig. 6 (d), we find that DiCNet also reduces the false negative rate, e.g., the wheels of the yellow muck truck are regarded as normal by MSP and SynthCP, while DiCNet predicts the correct anomaly score for the wheels.

### 4.4 Discussions

In this section, we report several variations of DiCNet and discuss their influences on anomaly discovery. Note that, all the following experiments adopt ResNet-50 based PSPNet (without the semantic classification head) as the teacher branch.

**Effect of Model Size.** As we discussed in Sec. 3.3, DiCNet is flexible in architecture design, we can distill the knowl-

| Backbone   | Epoch | AUPR $\uparrow$ | FPR95 $\downarrow$ | AUROC $\uparrow$ | Time    |
|------------|-------|-----------------|--------------------|------------------|---------|
| ResNet-101 | 10    | 11.6            | 27.5               | 88.3             | 450.2ms |
|            | 25    | <b>15.8</b>     | 18.7               | 93.1             |         |
|            | 50    | 15.6            | 20.8               | 92.2             |         |
|            | 110   | 14.7            | 24.0               | 90.9             |         |
| ResNet-50  | 3     | 12.5            | 19.7               | 92.5             | 347.8ms |
|            | 4     | 14.1            | 20.7               | 92.3             |         |
|            | 5     | 15.4            | 20.4               | 92.4             |         |
|            | 10    | 14.2            | 22.3               | 91.5             |         |
|            | 50    | 14.9            | 26.1               | 89.9             |         |
|            | 110   | 12.2            | 28.3               | 88.6             |         |
| ResNet-34  | 10    | 10.6            | 18.7               | 92.5             | 303.6ms |
|            | 50    | 13.8            | <b>18.1</b>        | 93.1             |         |
|            | 100   | 15.2            | 18.5               | 92.9             |         |
|            | 110   | 15.6            | <b>18.0</b>        | <b>93.3</b>      |         |
| ResNet-18  | 10    | 11.5            | 19.0               | 92.5             | 261.7ms |
|            | 50    | 14.4            | 18.8               | 93.0             |         |
|            | 100   | <b>15.8</b>     | 18.2               | <b>93.2</b>      |         |
|            | 110   | <b>15.7</b>     | 18.5               | 93.1             |         |
| VGG-19     | 20    | 8.9             | 23.5               | 90.4             | 242.5ms |
|            | 50    | 11.8            | 22.9               | 90.9             |         |
|            | 80    | 14.1            | 21.1               | 92.0             |         |
|            | 110   | 13.9            | 21.6               | 91.7             |         |
| AlexNet    | 20    | 9.2             | 23.3               | 90.8             | 236.4ms |
|            | 50    | 10.1            | 22.9               | 91.1             |         |
|            | 80    | 10.6            | 22.7               | 91.2             |         |
|            | 110   | 10.8            | 22.7               | 91.3             |         |

Table 4: Results of different backbones for student branch on StreetHazards. Note that ‘Time’ in the last column indicates the total inference time of DiCNet, not the student branch.

edge of the fixed teacher branch to any model size. To verify such a claim, we conduct experiments to study the effect of different model sizes of the student branch. Several key results are reported in Tab. 4. As we can see, the accuracy of different ResNet based backbone is closed to each other. e.g., ResNet-101 and ResNet-18 both obtain an AUPR score of 15.8. ResNet-34 achieves the best results in both FPR95 and AUROC. ResNet-101, ResNet-50 and ResNet-18 can also produce comparable results in these two metrics. However, a key mechanism of DiCNet is that different backbone has a different convergence speed. As seen in Tab. 4, ResNet-50 achieves its best results at epoch 5. Similarly, the best results of ResNet-101 is acquired at epoch 25. In contrast, if the backbone of the student branch is smaller than the teacher branch, more training epochs are demanded to ensure the consistency of the teacher branch and the student branch, e.g., for ResNet-34 and ResNet-18, we need more than 100 epochs to achieve their best results. Similar phenomenon can also be observed in VGG-19 and AlexNet. In addition, Tab. 4 also reported the inference time of DiCNet. By jointly considering the accuracy, the convergence speed and the inference time, we report the ResNet-34 based DiCNet as the best trade-off result.

#### 4.5 Failure Cases Analysis

As demonstrated in previous experiments, DiCNet performs well in most cases of detecting anomalies. However, it still fails in several challenging cases, mainly including seri-

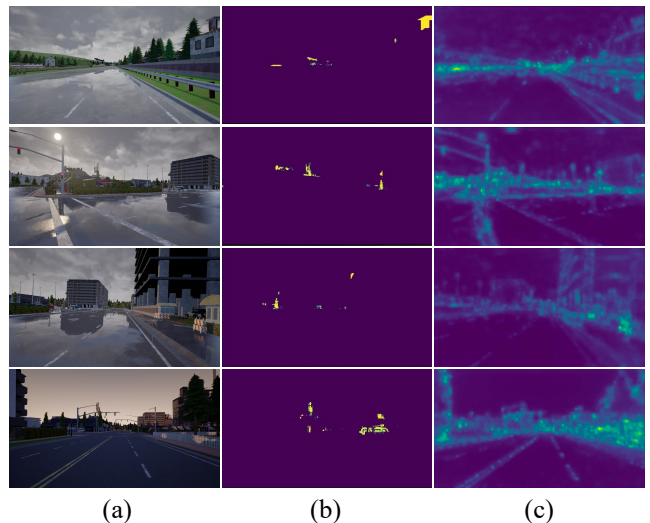


Figure 7: Some failure examples. (a) the input images, (b) ground truth of anomaly, (c) the anomaly score maps. Best view in color.

ous occlusion and small objects. Some failure examples are given in Fig. 7. DiCNet also has some false positives on some rarely seen normal objects. Note that all these errors are common challenges for the other state-of-the-art methods. We will try to address these issues in our further works.

## 5 Conclusion

This paper proposes a novel Distillation Comparison Network (DiCNet) for anomaly discovery in semantic segmentation, which contains a teacher branch and a student branch. The former one is trained under the common setting of semantic segmentation, the latter one is distilled from the fixed teacher branch through a distribution distillation. We leverage the discrepancy of the semantic feature between the two branches to discover the anomalies. DiCNet alleviates the issue caused by incorrect semantic classification efficiently. We conduct extensive experiments on two challenging datasets to verify the effectiveness of DiCNet.

## References

- Akay, S.; Atapour-Abarghouei, A.; and Breckon, T. P. 2018. Ganomaly: Semi-supervised anomaly detection via adversarial training. In *Asian Conference on Computer Vision*, 622–637.
- Badrinarayanan, V.; Kendall, A.; and Cipolla, R. 2017. Segnet: A deep convolutional encoder-decoder architecture for image segmentation. *IEEE Transactions on Pattern Analysis and Machine Intelligence*, 39(12): 2481–2495.
- Baur, C.; Wiestler, B.; Albarqouni, S.; and Navab, N. 2018. Deep autoencoding models for unsupervised anomaly segmentation in brain MR images. In *International MICCAI Brainlesion Workshop*, 161–169.
- Chen, L.-C.; Papandreou, G.; Kokkinos, I.; Murphy, K.; and Yuille, A. L. 2017. Deeplab: Semantic image segmentation

- with deep convolutional nets, atrous convolution, and fully connected crfs. *IEEE Transactions on Pattern Analysis and Machine Intelligence*, 40(4): 834–848.
- Cho, J. H.; and Hariharan, B. 2019. On the efficacy of knowledge distillation. In *International Conference on Computer Vision*, 4794–4802.
- Corbière, C.; Thome, N.; Bar-Hen, A.; Cord, M.; and Pérez, P. 2019. Addressing failure prediction by learning model confidence. In *Neural Information Processing Systems*, 2898–2909.
- Creusot, C.; and Munawar, A. 2015. Real-time small obstacle detection on highways using compressive RBM road reconstruction. In *Intelligent Vehicles Symposium*, 162–167.
- Deng, J.; Dong, W.; Socher, R.; Li, L.-J.; Li, K.; and Fei-Fei, L. 2009. Imagenet: A large-scale hierarchical image database. In *Computer Vision and Pattern Recognition*, 248–255.
- Di Biase, G.; Blum, H.; Siegwart, R.; and Cadena, C. 2021. Pixel-wise Anomaly Detection in Complex Driving Scenes. In *Computer Vision and Pattern Recognition*, 16918–16927.
- Fontanel, D.; Cermelli, F.; Mancini, M.; and Caputo, B. 2021. Detecting anomalies in semantic segmentation with prototypes. In *Computer Vision and Pattern Recognition*, 113–121.
- Franchi, G.; Bursuc, A.; Aldea, E.; Dubuisson, S.; and Bloch, I. 2020. TRADI: Tracking deep neural network weight distributions. In *European Conference on Computer Vision*.
- Gal, Y.; and Ghahramani, Z. 2016. Dropout as a bayesian approximation: Representing model uncertainty in deep learning. In *International Conference on Machine Learning*, 1050–1059.
- Geifman, Y.; and El-Yaniv, R. 2017. Selective classification for deep neural networks. *arXiv preprint arXiv:1705.08500*.
- Geng, Q.; Zhang, H.; Qi, X.; Huang, G.; Yang, R.; and Zhou, Z. 2021. Gated path selection network for semantic segmentation. *Transactions on Image Processing*, 30: 2436–2449.
- Hendrycks, D.; Basart, S.; Mazeika, M.; Mostajabi, M.; Steinhardt, J.; and Song, D. 2019. A benchmark for anomaly segmentation. *arXiv preprint arXiv:1911.11132v1*.
- Hendrycks, D.; and Gimpel, K. 2017. A baseline for detecting misclassified and out-of-distribution examples in neural networks. In *International Conference on Learning Representations*.
- Hinton, G.; Vinyals, O.; and Dean, J. 2015. Distilling the knowledge in a neural network. *arXiv preprint arXiv:1503.02531*.
- Izmailov, P.; Podoprikin, D.; Garipov, T.; Vetrov, D.; and Wilson, A. G. 2018. Averaging weights leads to wider optima and better generalization. In *Uncertainty in Artificial Intelligence*, 876–885.
- Janai, J.; Güney, F.; Behl, A.; Geiger, A.; et al. 2020. Computer vision for autonomous vehicles: Problems, datasets and state of the art. *Foundations and Trends® in Computer Graphics and Vision*, 12(1–3): 1–308.
- Jiang, H.; Kim, B.; Guan, M. Y.; and Gupta, M. R. 2018. To trust or not to trust a classifier. In *Neural Information Processing Systems*, 5546–5557.
- Komodakis, N.; and Zagoruyko, S. 2017. Paying more attention to attention: improving the performance of convolutional neural networks via attention transfer. In *International Conference on Learning Representations*.
- Lakshminarayanan, B.; Pritzel, A.; and Blundell, C. 2017. Simple and scalable predictive uncertainty estimation using deep ensembles. In *Neural Information Processing Systems*, 6402–6413.
- Lis, K.; Nakka, K.; Fua, P.; and Salzmann, M. 2019. Detecting the unexpected via image resynthesis. In *International Conference on Computer Vision*, 2152–2161.
- Liu, F.; Xia, Y.; Yang, D.; Yuille, A. L.; and Xu, D. 2019. An alarm system for segmentation algorithm based on shape model. In *International Conference on Computer Vision*, 10652–10661.
- Maddox, W. J.; Izmailov, P.; Garipov, T.; Vetrov, D. P.; and Wilson, A. G. 2019. A simple baseline for bayesian uncertainty in deep learning. In *Neural Information Processing Systems*, 13132–13143.
- Munawar, A.; Vinayavekkin, P.; and De Magistris, G. 2017. Limiting the reconstruction capability of generative neural network using negative learning. In *International Workshop on Machine Learning for Signal Processing*, 1–6.
- Phuong, M.; and Lampert, C. H. 2019. Distillation-based training for multi-exit architectures. In *International Conference on Computer Vision*, 1355–1364.
- Romero, A.; Ballas, N.; Kahou, S. E.; Chassang, A.; Gatta, C.; and Bengio, Y. 2014. Fitnets: Hints for thin deep nets. *arXiv preprint arXiv:1412.6550*.
- Schlegl, T.; Seeböck, P.; Waldstein, S. M.; Schmidt-Erfurth, U.; and Langs, G. 2017. Unsupervised anomaly detection with generative adversarial networks to guide marker discovery. In *International Conference on Information Processing in Medical Imaging*, 146–157.
- Tung, F.; and Mori, G. 2019. Similarity-preserving knowledge distillation. In *International Conference on Computer Vision*, 1365–1374.
- Vyas, A.; Jammalamadaka, N.; Zhu, X.; Das, D.; Kaul, B.; and Willke, T. L. 2018. Out-of-distribution detection using an ensemble of self supervised leave-out classifiers. In *European Conference on Computer Vision*, 550–564.
- Wang, T.-C.; Liu, M.-Y.; Zhu, J.-Y.; Tao, A.; Kautz, J.; and Catanzaro, B. 2018. High-resolution image synthesis and semantic manipulation with conditional gans. In *Computer Vision and Pattern Recognition*, 8798–8807.
- Xia, Y.; Zhang, Y.; Liu, F.; Shen, W.; and Yuille, A. L. 2020. Synthesize then compare: Detecting failures and anomalies for semantic segmentation. In *European Conference on Computer Vision*, 145–161.
- Xie, Q.; Luong, M.-T.; Hovy, E.; and Le, Q. V. 2020. Self-training with noisy student improves imagenet classification. In *Computer Vision and Pattern Recognition*, 10687–10698.

- Yang, C.; Xie, L.; Qiao, S.; and Yuille, A. L. 2019. Training deep neural networks in generations: A more tolerant teacher educates better students. In *AAAI Conference on Artificial Intelligence*, volume 33, 5628–5635.
- Yim, J.; Joo, D.; Bae, J.; and Kim, J. 2017. A gift from knowledge distillation: Fast optimization, network minimization and transfer learning. In *Computer Vision and Pattern Recognition*, 4133–4141.
- Yu, F.; Chen, H.; Wang, X.; Xian, W.; Chen, Y.; Liu, F.; Madhavan, V.; and Darrell, T. 2020. Bdd100k: A diverse driving dataset for heterogeneous multitask learning. In *Computer Vision and Pattern Recognition*, 2636–2645.
- Yuan, Y.; and Wang, J. 2018. Ocnet: Object context network for scene parsing. *arXiv preprint arXiv:1809.00916*.
- Zhang, Y.; Xiang, T.; Hospedales, T. M.; and Lu, H. 2018. Deep mutual learning. In *Computer Vision and Pattern Recognition*, 4320–4328.
- Zhao, H.; Shi, J.; Qi, X.; Wang, X.; and Jia, J. 2017. Pyramid scene parsing network. In *Computer Vision and Pattern Recognition*, 2881–2890.